Materiales de Construcción 74 (356)
October-December 2024, e360
ISSN-L: 0465-2746, eISSN: 1988-3226
https://doi.org/10.3989/mc.2024.390924

Valorization of phosphate by-products to produce acidic geopolymers

S. En-naji[a], S. Chhaiba[b], S. Mabroum[a], R. Hakkou[a,c] , I. Garcia Lodeiro[b]✉

[a] Cadi Ayyad University (UCA), Faculty of Science and Technology, IMED-Lab, (Marrakech, Morocco)
[b] Eduardo Torroja Institute (IETcc-CSIC), Department of Materials, (Madrid, Spain)
[c] Mohammed VI Polytechnic University (UM6P), Geology & Sustainable Mining Institute (GSMI), (Benguerir, Morocco)
✉: iglodeiro@ietcc.csic.es

Received 24 July 2024
Accepted 9 October 2024
Available on line 23 January 2025

ABSTRACT: The present study evaluates the possibility of using a by-product of phosphate mines, such as red clay, as a precursor for the elaboration of acid geopolymers, using H_3PO_4 phosphoric acid (5M and 8M) as an activator. Considering the chemical composition of the clay, sodium aluminate ($NaAlO_2$) was added as an aluminum corrector. To increase the reactivity of the precursor, the clay was thermally treated at 900°C for 2 hours. Pastes were prepared and characterized from the mechanical (compressive strengths), microstructural (BSEM/EDX and MIP), mineralogical (XRD and FTIR), and nanostructural (^{27}Al, ^{29}Si and ^{31}P MAS NMR) point of view. The results showed that the type of reaction products is highly dependent on the chemical composition of the precursor and the acidic conditions. In addition, the presence of sodium aluminate improves the mechanical strengths in systems activated with 8M H_3PO_4.

KEY WORDS: Geopolymers; Phosphate mining; Phosphoric acid; Red clay.

Citation/Citar como: En-naji S, Chhaiba S, Mabroum S, Hakkou R, Garcia Lodeiro I. 2024. Valorization of phosphate by-products to produce acidic geopolymers. Mater. Construcc. 74(356):e360. https://doi.org/10.3989/mc.2024.390924.

RESUMEN: *Valorización de subproductos de minas de fosfato para producir geopolímeros ácidos.* En el presente estudio se evalúa la posibilidad de emplear un subproducto de minas de fosfato, tales como la arcilla roja, como precursor a la hora de elaborar geopolímeros ácidos, empleando como activador, ácido fosfórico H_3PO_4 (5M y 8M). Considerando la composición quimica del precursor de partida (la arcilla roja), se empleó como corrector de aluminio, aluminato sódico ($NaAlO_2$). Con el fin de aumentar la reactividad de la arcilla, esta se activó térmicamente a 900°C durante 2 horas. Con los materiales anteriormente mencionados (la arcilla deshidroxilada y el H_3PO_4) se prepararon pastas se caracterizaron desde el punto de vista mecánico (resistencias a compresión), microestructural (BSEM/EDX y Porosimetia de Intrusión de Mercurio), mineralógico (DRX y FTIR) y nanoestructural (^{27}Al, ^{29}Si y ^{31}P NMR-MAS). Los resultados obtenidos manifiestan que el tipo de productos de reacción generados depende en gran medida de la composición química del precursor y de las condiciones de activación ácidas. Además, la incorporación de aluminato sódico mejora las resistencias mecánicas en los sistemas activados con 8M H_3PO_4.

PALABRAS CLAVE: Geopolímeros; Minas de fosfato; Ácido fosfórico; Arcilla roja.

1. INTRODUCTION

Nowadays, scientific researchers are increasingly looking for optimal solutions that simultaneously mitigate the negative impact of industrial waste and produce ecological materials that contribute to environmental protection. One example of this is the alkaline cements also known as geopolymers, which are recognized as sustainable materials, usually made with secondary by-products as precursors (such as blast furnace slags or coal fly ash), and alkaline sources as an activator. These can play an important role in many fields such as the construction industry, immobilization of hazardous materials, adsorption of contaminants from wastewater, etc. (1–3). Geopolymers have always attracted the interest of researchers for their potential to decrease the carbon dioxide emissions associated with cement production, offering a viable alternative (4). Historically, these materials were known first as alkali-activated materials. These materials have proven not only to be more sustainable from an environmental point of view, but also to have similar or even superior strength and technological behavior to conventional cements, making them the object of various applications (4–6). Traditionally, these cements are generated by reacting an aluminosilicate precursor with an alkaline activating solution (sodium hydroxide, waterglass...), however, recent studies (7) have demonstrated the possibility of using acid solutions (phosphoric acid) generating materials with interesting properties, such as porous matrices capable of acting as immobilizing matrices for dyes or heavy metals (2), or materials for thermal insulation (8, 9). The reaction products of acidic geopolymers differ significantly from those of alkali-activated geopolymers due to the influence of the medium's pH. Generally, in alkaline geopolymers, the major reaction product is C-A-S-H gel (for high calcium content precursors), N-A-S-H gel (in low calcium content precursors). In hybrid systems, the product is a mixture of different types of gels (3, 10). For acidic geopolymers, the main reaction products depend on the nature and chemical composition of the precursor used. In this context, Li et al., used different mixtures of high-magnesium nickel slag (HMNS) and fly ash (FA) activated with H_3PO_4 (11). Their study focused on various curing methods: curing with fresh-keeping film, curing in water, curing in air, standard curing, and curing at constant temperatures. The curing time were 3, 7, and 28 days. The main reaction products identified were aluminophosphate gel, newberyite gel phase and crystals, and aluminum silicon phosphate gel phase and crystals. Alshaaer et al., conducted a study aimed at producing geopolymers activated with 10M H_3PO_4. The specimens were cured 24 h at 60 °C and then at room temperature for 28 days (12). The main reaction products were -Si-O-P-O-Si- with aluminum phosphate crystals. Lin et al., also studied the activation of metakaolin using H_3PO_4. The major structural units identified were Si-O-Si, Si-O-Al, Si-O-P, and Al-O-P. Moreover, Zhan et al., studied the activation of metakaolinite with H_3PO_4, incorporating Al_2O_3 powder into the mixture (13). The main reaction product in this case was Si-O-Al-O-P-O-. In summary, the type of reaction products generated is highly dependent on the nature of the precursor, the acid activator, and the activation conditions.

It is important to mention that most of these studies used precursors with low calcium content. This suggests that the reaction products in the present study will be significantly different because the precursor used is obtained from the wastes generated during phosphate ore extraction, which are rich in CaO. The use of industrial wastes as precursors for the production of geopolymers has attracted considerable research interest. Various wastes, including waste glass, fly ash, and mining wastes such as phosphate waste, have been tested for this purpose (3, 14).

Moroccan researchers have actively focused on valorizing phosphate mining wastes for various applications. These by-products have been successfully used in the formulation of concretes, fired bricks, mortars, and geopolymers with promising results (15–18). The use of such wastes in various applications can significantly reduce their negative environmental impact. Given the large quantities of phosphate mining waste typically deposited near mining sites, this practice often leads to serious environmental problems, including the degradation of the physical landscape and its aesthetic value (3).

The objective of the present work is to evaluate the potential of a secondary mine waste products (red clay) as a precursor for the elaboration of acid geopolymers, paying particular attention to the identification of the reaction products generated and trying to optimize the experimental conditions for the production of geopolymers from phosphate by-products. This approach will also help reduce the negative impacts of phosphate mine waste disposal.

2. MATERIALS AND METHODS

2.1. Characterization of the precursor (red clay)

A red clay, a by-product of phosphate mining, has been used as a precursor to prepare acidic geopolymers. The particle size distribution analysis (laser granulometry) was performed to investigate the fine-

ness of the clay under study. The particle size distribution is shown in Figure 1. The results show that 90%, 50%, and 10% of the clay particles have sizes smaller than 70.8 µm, 12.5 µm, and 1.60 µm, respectively.

The chemical composition (XRF analysis) is shown in Table 1. The results show that the major oxides are calcium oxide (32.53%), followed by silica (25.22%), magnesium oxide (11.44%), alumina (4.45%), and iron oxide (1.58%). The percentage of alumina is slightly low (lower than 5%). Figure 3(a) shows the XRD pattern of the red clay, where, a part of montmorillonite and other crystalline phases were detected (quartz, tridymite, dolomite, hematite, fluorapatite, and calcite).

Improving the reactivity of the clay before using it as a precursor for geopolymer production is a priority (19). TG/DTG analysis was performed to determine the appropriate dehydroxylation temperature. Figure 2 shows the TG/DTG curves where three distinct peaks can be observed. The first peak is attributed to water loss in the clay, which typically occurs around 100°C (3). The second peak, located around 550 °C, corresponds with the decomposition of dolomite (previously identified by XRD) to produce $CaCO_3$ + MgO. The third peak, located around 750°C, corresponds with the overlapping of several phenomena that occur in this temperature range, i) the dehydroxylation of montmorillonite, which typically occurs at 700°C (20) and ii) the decomposition of calcite (both the one identified in XRD and the one originated in the decomposition of $CaMg(CO_3)_2$) to produce lime (CaO) (21).

XRD and FTIR were performed after the thermal treatment process (see Figures 3(a) and (b) respectively. Quartz (SiO_2), tridymite (SiO_2), fluorapatite ($Ca_5(PO_4)_3F$), and hematite (Fe_2O_3) remain present after the thermal treatment, indicating that they were not affected by the high temperature (900°C for 2 hours). Lime (CaO) and periclase (MgO) are formed due to the decomposition of dolomite. The disappearance of calcite ($CaCO_3$) is also due to its decarbonation to lime. In addition, the thermal treatment of clay minerals and dolomite leads to the crystallization of gehlenite ($Ca_2Al(AlSiO_7)$) and diopside ($CaMgSi_2O_6$), where the diopside is known by its formation at the dolomite/quartz interface (the crystallization of these phases could detract from the reactivity of the precursor). FTIR results for the raw clay before and after thermal treatment are shown in Figure 3-b. The band that appears after thermal treatment at 3643 cm^{-1} is attributed to the asymmetric stretching of hydroxyl bonds in portlandite. However, this phase was

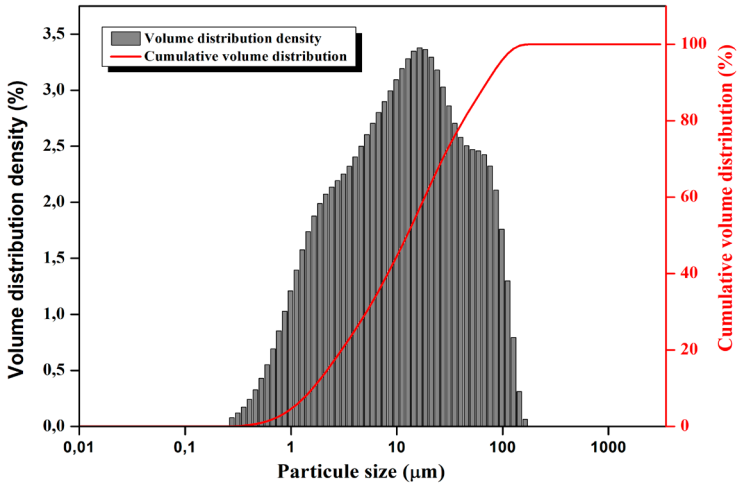

Figure 1. Particle size distribution of red clay.

Table 1. Chemical composition of the red clay (XRF, % oxides in weight).

Chemical composition wt.%	LOI	CaO	SiO_2	MgO	Al_2O_3	Fe_2O_3	P_2O_5	TiO_2	K_2O	Na_2O
Red clay	23.63	32.53	25.22	11.44	4.45	1.58	0.39	0.24	0.20	0.11

LOI: Loss of ignition at 1000°C

not detected in the XRD pattern suggesting that it is present in small amounts or was not very well crystallized. The two bands at 1635 cm^{-1}, and 3435 cm^{-1} characterize the deformation and stretching vibrations of the O-H and H-O-H bonds, respectively. It is important to note that these two bands also appear in the spectra after thermal treatment. This could be explained by the fact that water was re-adsorbed during the experimental procedure. The bands at 2924, 2521, 1431, 876, 728, and 712 cm^{-1} indicate the presence of carbonates, which disappear after thermal treatment except the band at 1431 cm^{-1} has not completely disappeared, indicating that the carbonation process was not complete. The doublet appearing around 796 cm^{-1}, as well as the band at 471 cm^{-1}, characterize Si-O-Si bond deformation vibrations in quartz that still appear after thermal treatment, which is in good agreement with previous findings. The clay Al-O, Si-O-Si, and Si-O groups are characterized by the band at 1041 cm^{-1}, which shifts from 1091 cm^{-1} due to chemical and structural changes (22). The peak at 523 cm^{-1} is attributed to deformation vibrations of Al-O (22). The band at 917 and 876 cm^{-1} which characterizes the presence of Al-O-H and Al-OH-Al respectively, can also confirm the dehydroxylation of montmorillonite with its disappearance after thermal treatment (23).

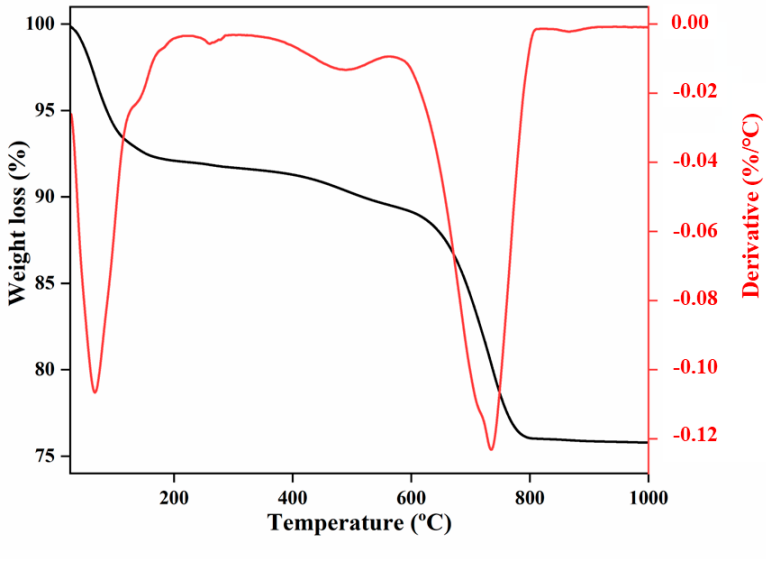

Figure 2. TG/DTG analysis of raw clay.

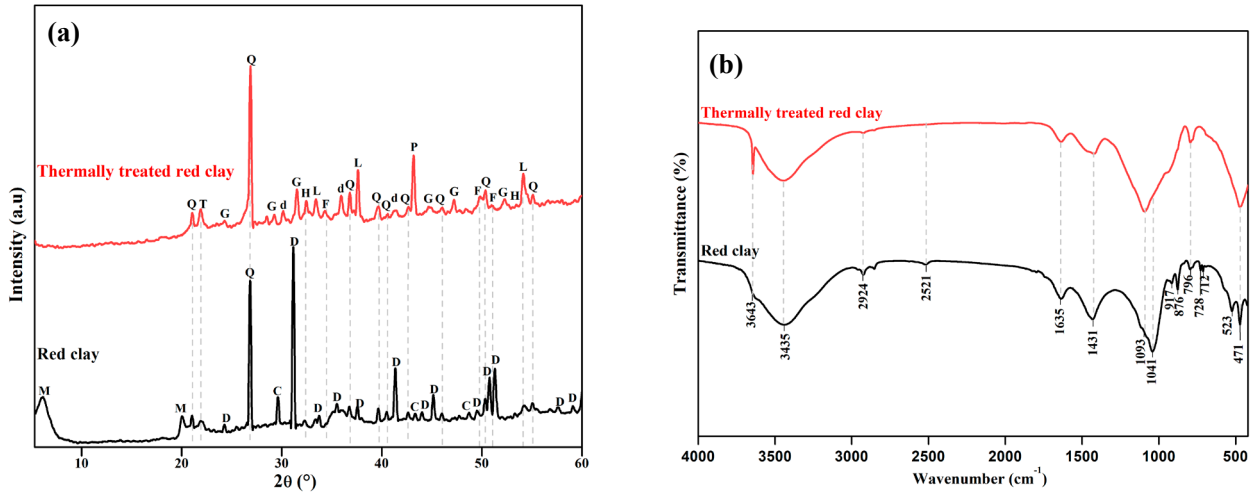

Figure 3. XRD (a) and FTIR (b) analyses of red clay before and after the thermal treatment (M: Montmorillonite (COD9002779), Q: Quartz (COD1011159), T: Tridymite (COD9013393), D: Dolomite (COD1200014), C: Calcite (COD1010928), L: Lime (COD1011095), H: Hematite (COD1011267), d: diopside (COD1011057), P: Periclase (COD9006747), F: Fluorapatite (COD9010504), G: Gehlenite (COD9006113)).

Figure 4 shows the ^{27}Al and ^{29}Si NMR spectra of the clay after the thermal treatment. ^{27}Al NMR spectrum shows a broad peak at about +50.16 ppm, which is attributed to 4-coordinated aluminum, corresponding with the conversion of Al(VI) to Al(IV) in montmorillonite after the thermal activation (24). According to A. Noushini et al., the peak associated with Al(IV) in gehlenite appears around +66 ppm; however, this signal overlaps with other Al(IV) signals in the broad peak observed at +50.16 ppm (25). The small shoulder at about +10.2 ppm is associated with 6-coordinated aluminum, indicating that the montmorillonite has not been completely dehydroxylated (26). ^{29}Si MAS NMR was also utilized to investigate silicate structures. The resonance at -72.2 ppm is attributed to $Q^1(3Al)$ sites present in gehlenite (27). The resonance at -84.3 ppm corresponds to diopside (28). Moreover, the peak at -103.9 ppm indicates the presence of Q^4-type species associated with the calcined montmorillonite (24). In addition, the two peaks at -108.1 ppm and -113.0 ppm are attributed to Q^4 sites present in quartz and tridymite, respectively (3, 29).

2.2. Experimental

2.2.1. Preparation of the red clay based geopolymers

After the thermal treatment of the clay, to be used as a precursor, the next step was the preparation of the acid geopolymers. For that phosphoric acid was chosen as an activator and used in different concentrations (5M and 8M) to study its influence on the final product. Considering the small proportion of aluminum in the precursor, since aluminum plays a significant role in the geopolymerization process, an additional source of aluminum (sodium aluminate, $NaAlO_2$) was incorporated into the pastes in varying proportions to study its effect on the geopolymers.

Six formulations, varying in the proportions of red clay and sodium aluminate, were prepared by acid activation with 5M and 8M H_3PO_4. The molar concentrations were chosen based on preliminary tests and previous studies. Similar procedures as the one taken by Tchakouté et al., were followed and various preliminary tests were conducted to determine the appropriate concentrations for the activator (30). Tchakouté et al., investigated the effect of phosphoric acid concentration on geopolymer properties using metakaolin as the only precursor and tested concentrations of 4, 6, 8, 10, 12, and 14M. Their results showed that geopolymers activated with 10M H_3PO_4 had the highest compressive strength. In this study, however, due to workability considerations, only geopolymer pastes activated with 5M and 8M H_3PO_4 were selected for study.

Table 2 shows the dosification for each type of geopolymer. The appropriate liquid/solid (L/S) ratios have been determined based on some preliminary tests that consist in maintaining the same workability in all pastes. All formulations were prepared under identical conditions. Mixing time was set at 3 minutes, and the pastes obtained were poured into prismatic molds of 1 x 1 x 6 cm^3 and cured in an oven at 70°C for 72 hours. After this temperature curing, the paste specimens were sealed in plastic film and place in the leave in the laboratory (21°C) until compression tests were performed at 7, 28, and 90 days. One piece of the untested specimen was kept for microstructural characterization (BSEM and MIP), while the rest was ground and used for mineralogical and nanostructural analysis (FTIR, XRD and NMR). At selected ages the

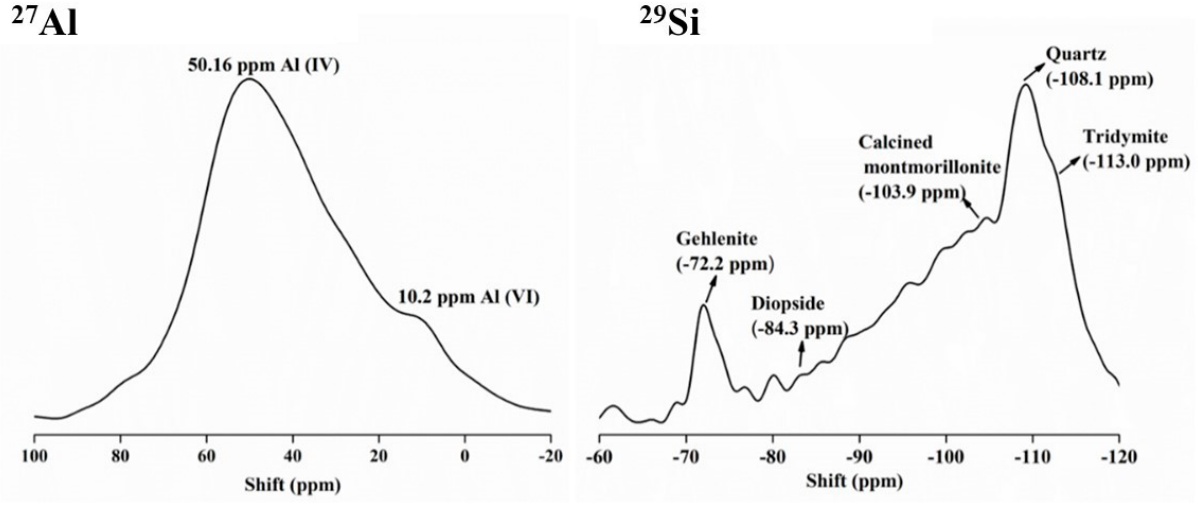

Figure 4. ^{27} Al and ^{29} Si NMR spectra of the thermally treated red clay (T-RC).

Table 2. Main feature of the pastes.

Geopolymer	T-RC* (%) (solid)	$NaAlO_2$* (%) (solid)	H_3PO_4 concentration (M) (liquid)	L/S ratio[1]
GP-5% $NaAlO_2$ -5M H_3PO_4 (GP-1)	95	5	5	1.3
GP-10% $NaAlO_2$ -5M H_3PO_4 (GP-2)	90	10	5	1.3
GP-15% $NaAlO_2$ -5M H_3PO_4 (GP-3)	85	15	5	1.3
GP-5% $NaAlO_2$ -8M H_3PO_4 (GP-4)	95	5	8	1.1
GP-10% $NaAlO_2$ -8M H_3PO_4 (GP-5)	90	10	8	1.1
GP-15% $NaAlO_2$ -8M H_3PO_4 (GP-6)	85	15	8	1.1

(*) weight %; (1) liquid solid ratio

collected specimens were immersed in isopropanol for 24 hours to stop the geopolymerization reaction, to then be dried in a desiccator during 48 hours.

2.2.2. Methods

Compressive strength tests were performed using an Ibertest Autotest 200/-10-SW press. Mercury intrusion porosimetry (MIP) was used to study changes in the pore structure of the prepared geopolymers using an AutoPore IV 9500 V1.09 Serial 293 porosimeter from Micromeritics Instrument Corporation. A Bruker D8 Advance diffractometer was used to study the mineralogy of the clay before and after the thermal treatment as well as after acid activation, operating in the 2θ range of 5-60° with a step size of 0.02° every 0.5 s using CuKα radiation at 40 kV and 30 mA. FTIR analysis was performed to investigate the functional groups of the samples using a Thermo Scientific NICOLET 600 FT-IR spectrophotometer, with spectra collected in the 4000-400 cm-1 range. The microstructure of a representative sample was studied using an S-4800 scanning electron microscope coupled to a HITACHI energy dispersive X-ray spectrometer, and the data were processed using Bruker ESPRIT 2 software.

The Magic Angle Spinning Nuclear Magnetic Resonance (MAS-NMR) spectroscopy was carried out to analyze solid-state ^{27}Al – ^{29}Si – ^{31}P using a Bruker AVANCE II 400WB instrument. For ^{29}Si NMR spectra, data were collected at 79.5 MHz with a π/2 pulse width of 5 μs and a relaxation delay of 10s. The spectra were referenced to Tetramethylsilane (TMS). Meanwhile, the resonance frequency of ^{27}Al was 104.3 MHz, and a π/2 pulse technique of 5 μs was applied with a delay of 10 s. Chemical shifts were recorded relative to external Al $(H_2O)_6^{3+}$. High resolution ^{31} P-MAS and ^{31} P{^{1}H} CP-MAS spectra were recorded at 161.98 MHz (9.4 T magnetic field) by spinning the samples at the magic angle (54º44'').

The ^{31}P-MAS spectra were obtained after a π/2 excitations of 2.85 μs and intervals between successive accumulations of 60 s. The number of accumulations was 40. The 31 P{^{1} H} CP-MAS spectra were obtained with a contact time for cross polarization of 3 ms, intervals between successive accumulations of 5 s and the number of accumulations was 200. The ^{31}P chemical shift values are given relative to 85 % H_3PO_4 aqueous solution.

2.2.3. Limitations of some methods

The use of multiple analytical techniques is essential in the study of any material, as each method has its limitations. For example, XRD is valuable for determining the mineralogical composition of materials, but the presence of overlapping diffraction peaks can make it difficult to identify minor phases. To complement and confirm the XRD results, FTIR was also used to identify the functional groups in the samples. However, FTIR is very sensitive to moisture, and overlapping peaks can make it difficult to accurately assign functional groups. In addition, improper sample preparation can affect peak quality, which must be taken into account when interpreting the results. NMR analysis has been used to complement the previous techniques by investigating the Al, Si, and P environments and providing detailed structural information. However, NMR also has limitations, such as noise in the spectra due to the sensitivity of the technique, which can complicate deconvolution and interpretation of the results. In summary, the use of several techniques allows us to have a more accurate interpretation of the results.

3. RESULTS AND DISCUSSION

Figure 5 shows the compressive strength values for geopolymers activated with 5M and 8M H_3PO_4

solution after 7, 28, and 90 days of curing. It is distinguished that the strength development is highly dependent on the H_3PO_4 concentration. The systems with 8M H_3PO_4 develop higher strengths attaining 14.5 MPa at 90 days. The effect of phosphoric acid concentration on metakaolin-based geopolymers was previously studied by (30), in the acidic geopolymers prepared with different acid concentrations (4, 6, 8, 10, 12, and 14M) to study its effect on the properties of the final products. The results of this study showed that increasing the H_3PO_4 concentration from 4 to 10M increased the compressive strength values. This was explained by the presence of a small amount of free water remaining in the solution at low concentration values, that does not react during the geopolymerization process. This leads to the formation of pores when the specimens are dried, resulting in low compressive strength values, which was the case in the present study. In addition, the compressive strength values of geopolymers activated with 8M H_3PO_4 increase with the amount of $NaAlO_2$. After dissolution, $NaAlO_2$ provide tetrahedral aluminium, that can participate in the formation of reaction products (especially $AlPO_4$ and the amorphous gel, as it will be shown below), which could lead to increase the compressive strength values.

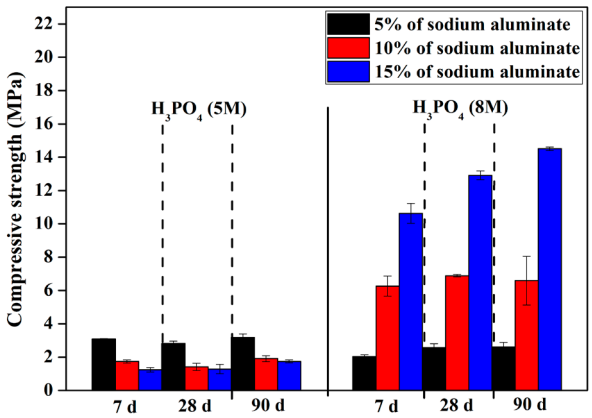

Figure 5. Compressive strength values of red clay based geopolymers activated with 5M and 8M H_3PO_4.

XRD analysis of both types of geopolymers (activated with 5 and 8 M H_3PO_4 acid) are shown in Figure 6. The results show the presence of certain phases, such as quartz and tridymite, that remained after acid activation (indicating that are not potentially reactive under these conditions). In addition, some new phases were formed due to the reaction between phosphoric acid and lime. Brushite ($CaHPO_4 \cdot 2H_2O$) appears as a new crystalline phase in geopolymers activated with 5 M phosphoric acid, while monetite ($CaHPO_4$) appears in those activated with 8 M. Monetite is the dehydrated phase of brushite (31). The formation of these phases depends highly on the pH values of the pore solution. According to the literature, monetite forms at pH values below 5 (32), while brushite forms at pH values below 6.5 (33). This implies that the pH for monetite formation is lower than that for brushite formation, which is consistent with the present study where the pH of 8M H_3PO_4 is lower than that of 5M H_3PO_4. It has also been reported by (34) that brushite cements have low compressive strength due to their rapid setting, resulting in poor crystal compaction during the setting process, which is in good agreement with the previous findings. In addition, newberyite ($MgHPO_4 \cdot 3H_2O$) and aluminum phosphate ($AlPO_4$) are present in both types of geopolymers. Notably, the crystallinity of newberyite is higher (much more sharp and defined peaks) in geopolymers activated with 5M phosphoric acid compared to those activated with 8M phosphoric acid. This suggests that newberyite may be present in both crystalline and amorphous forms in geopolymers activated with 8M phosphoric acid, potentially contributing to the higher compressive strength of these geopolymers. Moreover, the appearance of humps ranging from 18-40° indicates the formation of amorphous gels. Similar to the present study, the influence of phosphoric acid on the properties of geopolymers has been explored by several researchers, with a key difference being the type of precursor used. The study conducted by Pu *et al.,* demonstrated that when fly ash was activated with phosphoric acid, the crystalline reaction products were Berlinite, Monetite, and Brushite, while the amorphous phases included Si-O-Al-O-P, Si-O-P, and Al-O-P units (35). The highest compressive strength, 20 MPa, was achieved with 50% phosphoric acid (L/S = 0.3) after 90 days of curing. They noted that Berlinite enhances geopolymer strength and structure but may not support long-term strength growth in phosphate geopolymers. Similarly, Tchakouté et al., investigated metakaolin as a precursor activated by different concentrations of phosphoric acid and observed the formation of an amorphous phase (Si-O-P-O-Si) along with a crystalline phase (Berlinite) (30). The highest compressive strength was achieved with 10M phosphoric acid, and the presence of $AlPO_4$ was shown to enhance the overall strength. This emphasizes the key role aluminum content plays in precursor selection. Additionally, Riyap et al., reported that the formation of calcium phosphates in phosphoric acid-based geopolymers can reduce the amount of gel formed (36), resulting in lower compressive strength, which may explain the acceptable strength values obtained in the present study.

FTIR spectra are represented in Figure 7. The bands at 3411 cm^{-1} and 3485 cm^{-1} in the spectra of

both types of geopolymers (5 and 8M H_3PO_4) are associated with the stretching vibrations of the H-O-H bonds (2). The bands observed at 1650 cm^{-1} and 1649 cm^{-1} correspond to the deformation vibrations of O-H bonds. For the geopolymers activated with 5M H_3PO4, the presence of a broad band with two shoulder peaks at 1135 cm^{-1} and 1071 cm^{-1} indicates the presence of P-O bonds, characteristic of brushite (37). This is consistent with the XRD results, where brushite was noticeable in GP-5M but not in GP-8M. For the geopolymers activated with 8M H_3PO_4, the band shifts to a lower wavenumber (around 1081 cm^{-1}) and is associated with the formation of P–O–Al bonds (38). It is also important to note that these broad bands in both types of geopolymers could result from overlapping P-O bonds not only in crystalline phases, but also in amorphous phase that cannot be distinguished using XRD or FTIR. In addition, the bands around 976 cm^{-1} and 877 cm^{-1} are characteristic of P-OH bonds in newberyite, present in both types of geopolymers (39). The bands at 790 cm^{-1} and 794 cm^{-1} in the spectra of GP-5M and GP-8M, respectively, are characteristic of quartz, indicating that it was not by the acid activation (40). The band around 532 cm^{-1} can be attributed to the vibration modes of Al-O-P in ($AlPO_4 \cdot H_2O$) (41). Lastly, the band at 470 cm^{-1} is attributed to the vibration modes of Si-O-Si (42).

Since there is a tendency for the compressive strength values of GP-8M to increase with increasing sodium aluminate content, they were selected for further study. MIP analyses were performed on GP-8M and the results are shown in Figure 8. As expected for these acid geopolymers, the total porosity in the reference system was quite high (See Figure 8(a)). With

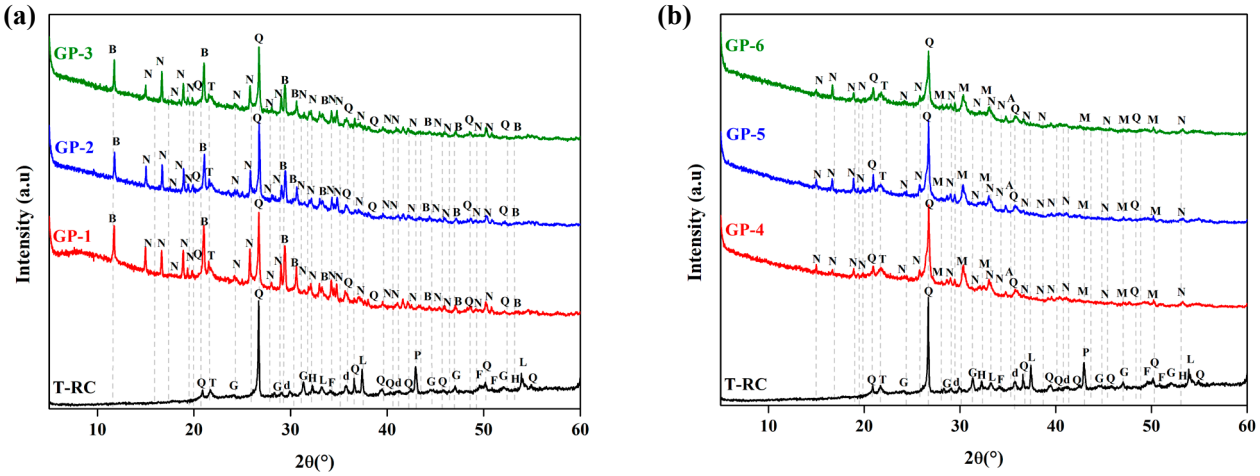

Figure 6. XRD patterns of geopolymers activated with (a) 5M H_3PO_4 and (b)geopolymers activated with 8M H_3PO_4 (Q: Quartz (COD1011159), T: Tridymite (COD9013393), L: Lime (COD1011095), H: Hematite (COD1011267), d: diopside (COD1011057), P: Periclase (COD9006747), F: Fluorapatite (COD9010504), G: Gehlenite (COD9006113), N: Newberyite (COD9014665), M: Monetite (COD9007619): A: Aluminum phosphate (COD9006404), B: Brushite (COD1533075)).

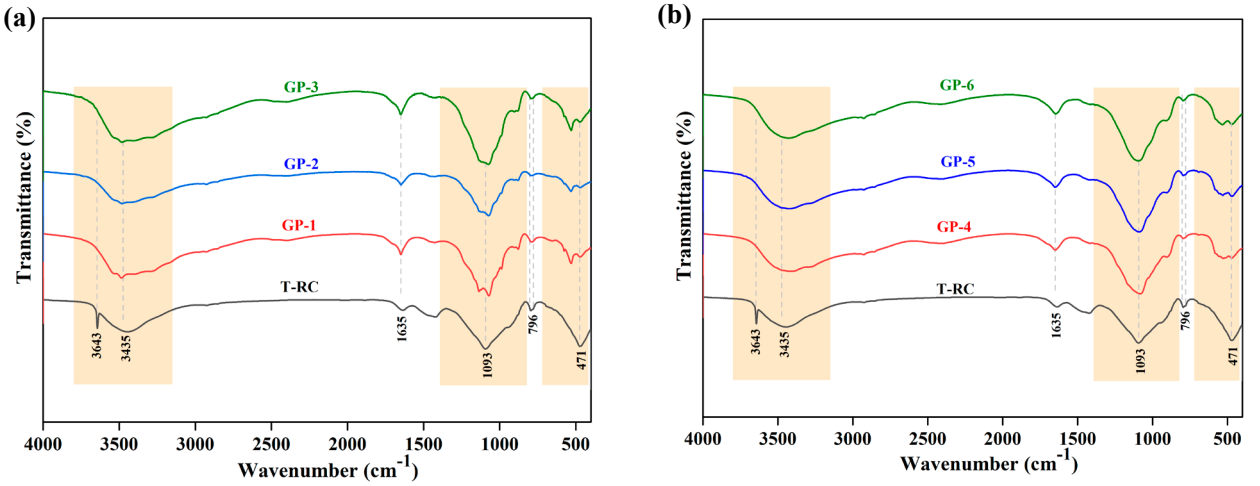

Figure 7. FTIR spectra of geopolymers activated with 5M H_3PO_4 (a) and geopolymers activated with 8M H_3PO_4 (b).

increasing amounts of $NaAlO_2$, the porosity decreases from 39.29% for the GP with 5% $NaAlO_2$ to 38.12% with 10% $NaAlO_2$ and to 34.09% with 15% $NaAlO_2$. In addition, there are changes in the pore size distribution towards smaller pore size diameter (See Figure 8(b). It can be observed that higher amounts of $NaAlO_2$ result in smaller pore diameter. Specifically, pore volume in the range of 10-100 microns decreases, while those in the range of 0.01-0.1 microns increase. The results obtained are in agreement with the compressive strength values (See Figure 5).

Geopolymers with high compressive strength values were selected as representative materials to be analyzed by BSEM after 28 days. The micrograph of the geopolymer containing 15% sodium aluminate and activated with 8M is shown in Figure 9. The microstructure shows a dense matrix where several phases can be distinguished. The same phases previously identified by XRD were also identified by EDS at various points, including quartz, monetite ($CaHPO_4$), aluminum phosphate ($AlPO_4$), and newberyite ($Mg(PO_3OH)\cdot 3H_2O$) were observed. The presence of unreacted remaining clay is also evident in the system, as some particles based on Si and Al are still present. In addition, the identification of a new phase can be distinguished, which could be related to the formation of an amorphous gel containing Si, Al, Ca, and P that can co-precipitate with the crystalline phases, in the acid system.

In order to explore the nanostructure of the reaction products, ^{27}Al, ^{29}Si, and ^{31}P MAS NMR analyses were conducted in a selected sample (geopolymers containing 15% $NaAlO_2$). In the same figure, the ^{27}Al and the ^{29}Si MAS NMR spectra of the thermal-

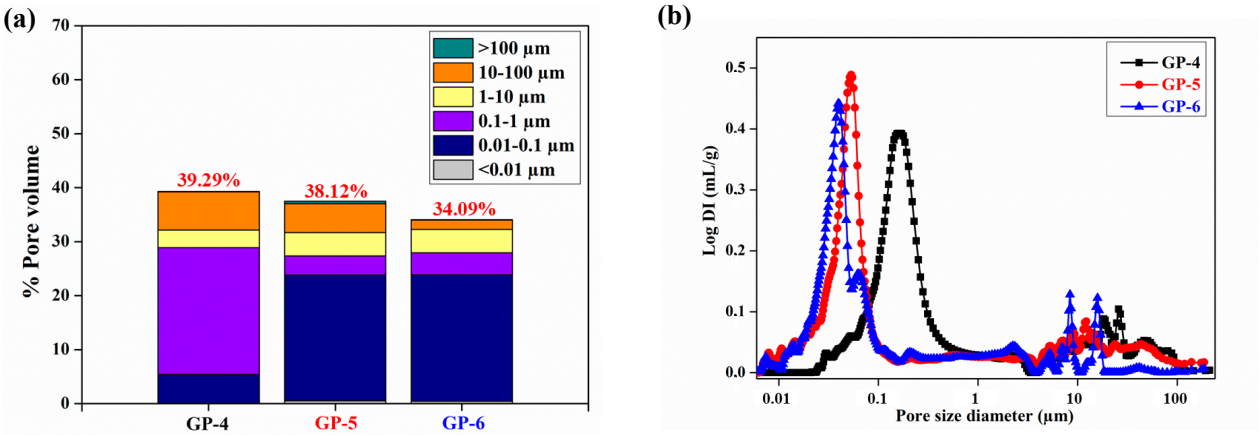

Figure 8. Total porosity of the geopolymers based on 8M (a) and the distribution of the pore size diameter (b).

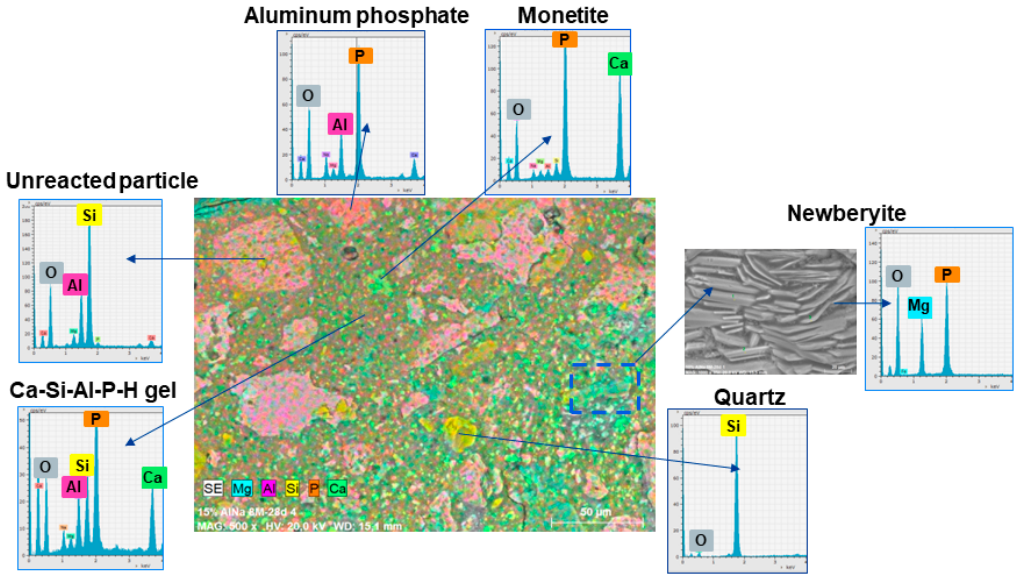

Figure 9. Mapping micrographs and EDS of GP-6.

ly treated clay have been including for comparative analysis. ^{29}Si NMR spectrum (see Figures 10(a) and 10(b)), shows the presence of one narrow peaks appearing at -72.8 ppm, that is attributed to the Q^1 sites of remaining gehlenite, (3). The identification of the peaks ranging from -82 ppm to -105 ppm is very challenging, and probably are the result of the overlapping of different Q^3(nAl)/Q^4(nAl) environments, that could correspond with unreacted particles clay's but also with the amorphous phase previously identified by BSEM. Additionally, the presence of quartz and tridymite (observed in XRD) is characterized by the two resonances at -109.1 ppm and -113.5 ppm, respectively (3). ^{27}Al NMR spectra of the geopolymer (GP-3) show resonances around +47.17, +8.11, and -13.88 ppm (Figure 10-c). The two first peaks are attributed to Al(IV) and Al(VI), respectively in the Si-O-Al-ordered structure (26). According to previous studies, the new peak at -13.88 ppm and the wide hump between +20 and +60 ppm are attributed to Al(VI)-OP and Al(IV)-OP structures coordinating with -O-Si and -OH to form the octahedral and tetrahedral structures ($Al(VI)(OP)_x(OSi)_y(OH)_{6-x-y}$) and ($Al(IV)(OP)_x(OSi)_y(OH)_{4-x-y}$) (43). Figure 10-d shows the deconvoluted ^{31}P NMR spectra of the sample GP-6 where several peaks can be distinguished. According to the literature, peaks at -0.3 and -1.5 ppm are attributed to the presence of monetite ($CaHPO_4$) (44). In the present study, two distinct peaks appeared at about -0.15 and -1.6 ppm, which could confirm the presence of monetite, previously identified by XRD. The signal at -7.4 ppm is attributed to the presence of newberyite (45). At about -13.9 ppm, the broad peak confirms the presence of aluminum phosphate (46). The formation of $AlPO_4$ can be classified into three types: surface precipitates (as in the case of aluminum phosphate resonating at -13 ppm), inner-sphere surface complexes where the resonance appears between -11 ppm and

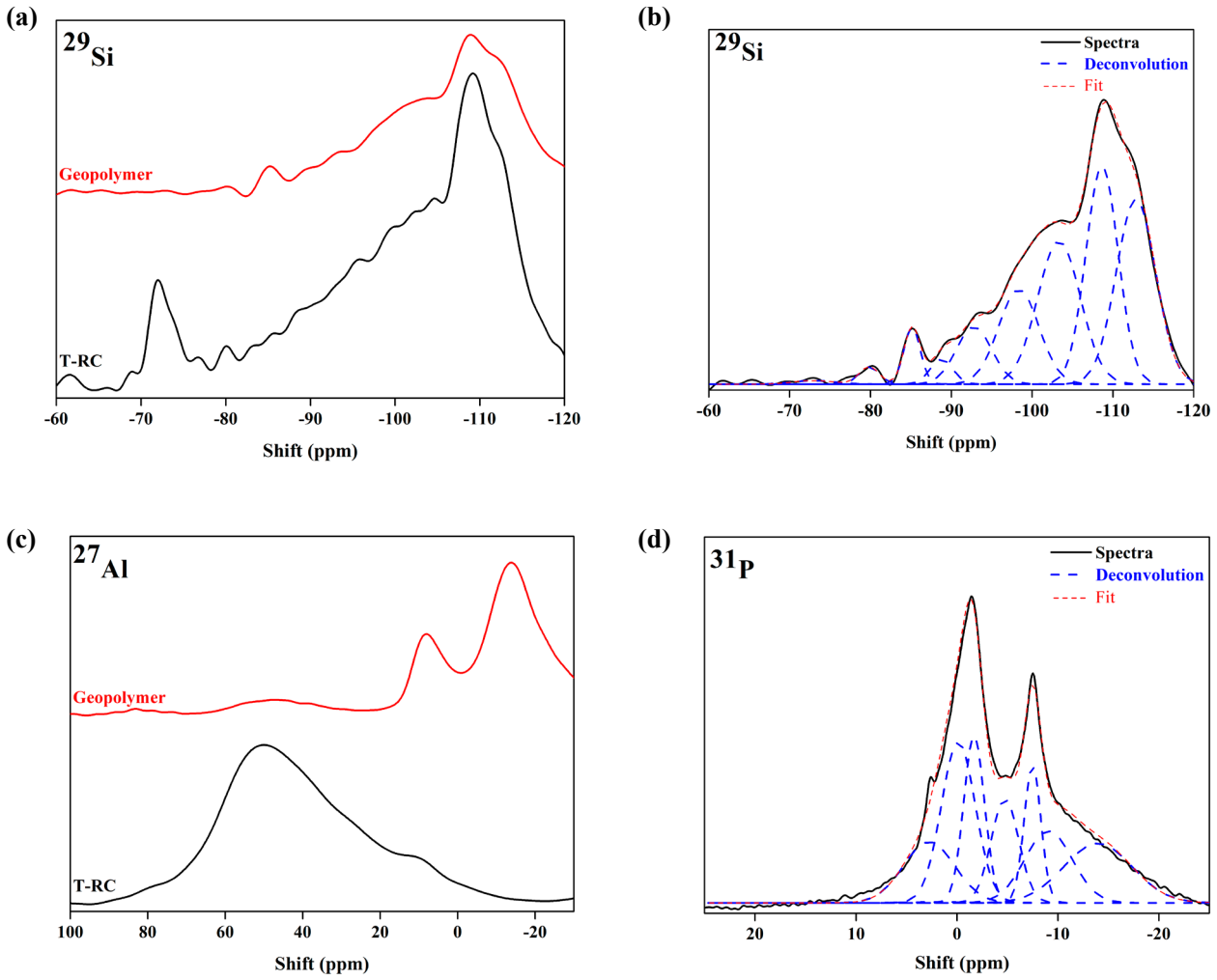

Figure 10. (a) ^{29}Si NMR spectra of geopolymer (GP-6) before and after activation, (b) Deconvoluted ^{29}Si NMR spectra of the GP-6, (c) ^{27}Al NMR spectra of geopolymers before and after activation, (d) Deconvoluted ^{31}P NMR spectra of GP-6.

0 ppm (as indicated by the bands appearing at -4.76 and -9.07 ppm), and outer-sphere types resonating between 0 ppm and 10 ppm (46). According to a previous study, the phosphorus environment of Q^0, generated by the orthophosphate group, corresponds to +2 ppm (13). Thus, the presence of peaks at about +1.7 and +2.8 ppm is attributed to the phosphorus environment of Q^0 (that could correspond with the formation of an amorphous phase containing P).

4. CONCLUSIONS

- Thermally treated red clay (a mine tailing waste) can be used as a precursor for the elaboration of acid geopolymers (set and harden developing acceptable strength (14.3 MPa/90days) and with a porosity that could be interesting for various applications (thermal insulation application, adsorption of contaminants from industrial wastewater, catalytic supports in chemical industry, lightweight materials, etc.).
- The type of reaction products obtained are highly dependent on the chemical composition of the precursor and the acidic conditions. It has been found that some reaction products vary depending on the concentration of phosphoric acid •
  The presence of sodium aluminate improves the mechanical strengths in systems activated with H_3PO_4 8M which means that Al^{3+} can participate in the formation of $AlPO_4$ and in the amorphous gel.
- An amorphous gel with a chemical composition based on Si, Al, Ca, and P has been detected. Further studies are needed to clarify the nanostructure of this phase. In addition, long-term durability studies, including resistance to chemical attack, and comprehensive environmental impact assessments should be conducted to ensure the material sustainability.
- Incorporating phosphate by-products into geopolymers production reduces both waste management and raw material costs, providing a more cost-effective solution for industries such as construction and wastewater treatment.

Funding Sources

The JIN project (PID2020-116738RJ-I0 AEI/10.13039/501100011033) and the RYC excellence contract (RYC2021-032620-I), funded by the Spanish Ministry of Science and Innovation (MCIN/AEI/10.13039/50110001033) and the European Union "Next generation EU/PRTR", are gratefully acknowledged. The authors also wish to express their appreciation to the Eduardo Torroja Institute collaborators in light of the ICOOP project 2022 (ref COOPA22026) as well as to Cadi Ayyad University's Center of Analysis and Characterization (CAC) for their valuable contribution to sample characterization tests.

¡Authorship contribution statement

Salma En-naji: Formal analysis, Research, Writing-original draft.

Salma Chhaiba: Formal analysis, Research.

Safaa Mabroum: Research.

Rachid Hakkou: Conceptualization, Supervision, Writing-review & editing.

Inés Garcia Lodeiro: Conceptualization, Formal analysis, Fund raising, Supervision, Writing-review & editing.

Declaration of competing interest

The authors of this article declare that they have no financial, professional or personal conflicts of in-terest that could have inappropriately influenced this work.

REFERENCES

1. Ain Jaya N, Yun-Ming L, Mustafa Al Bakri Abdullah M, Cheng-Yong H. 2019. Porous metakaolin geopolymers with tailored thermal conductivity. IOP Conf. Ser. Mater. Sci. Eng. 551:012088. http://doi.org/10.1088/1757-899X/551/1/012088
2. En-naji S, Ghazi S, Mabroum H, Mabroum S, Khatib K, Taha Y, Lodeiro IG, Hakkou R. 2023. Design of acid-geopolymers based on clays by-products for methylene blue removal from wastewater. Appl. Clay Sci. 245:107126. http://doi.org/10.1016/j.clay.2023.107126
3. Mabroum S, Garcia-Lodeiro I, Blanco-Varela M.T, Taha Y, Chhaiba S, Indris S, Benzaazoua M, Mansori M, Hakkou R. 2023. Formation of CSH and MSH gels in alkali-activated materials based on marl by-products from phosphate mines. Constr. Build. Mater. 365:130029. http://doi.org/10.1016/j.conbuildmat.2022.130029
4. Celerier H, Jouin J, Mathivet V, Tessier-Doyen N, Rossignol S. 2018. Composition and properties of phosphoric acid-based geopolymers. J. Non-Cryst. Solids. 493:94–98. http://doi.org/10.1016/j.jnoncrysol.2018.04.044
5. Palomo A, Maltseva O, Garcia-Lodeiro I, Fernández-Jiménez A. 2021. Portland versus alkaline cement: continuity or clean break: a key decision for global sustainability. Front. Chem. 9. http://doi.org/10.3389/fchem.2021.705475
6. Fernández-Jiménez A, Garcia-Lodeiro I, Maltseva O, Palomo A. 2023. Sustainable cements: hybrid alkaline cements overview. In Proceedings of the Proceedings of the 75th RILEM Annual Week 2021. Escalante-Garcia J.I. Castro Borges P. Duran-Herrera A. Eds, Springer International Publishing: Cham. pp. 626–639.

7. He M, Yang Z, Li N, Zhu X, Fu B, Ou Z. 2023. Strength microstructure CO_2 emission and economic analyses of low concentration phosphoric acid-activated fly ash geopolymer. Constr. Build. Mater. 374:130920. http://doi.org/10.1016/j.conbuildmat.2023.130920

8. Morsy MS, Rashad AM, Shoukry H, Mokhtar MM. 2019. Potential use of limestone in metakaolin-based geopolymer activated with H_3PO_4 for thermal insulation. Constr. Build. Mater. 229:117088. http://doi.org/10.1016/j.conbuildmat.2019.117088

9. Rashad AM, Gharieb M, Shoukry H, Mokhtar MM. 2022. Valorization of sugar beet waste as a foaming agent for metakaolin geopolymer activated with phosphoric Acid. Constr. Build. Mater. 344:128240. http://doi.org/10.1016/j.conbuildmat.2022.128240

10. Garcia-Lodeiro I, Fernández-Jiménez A, Palomo A. 2018. Hybrid alkaline cements: bentonite-opc binders. Minerals. 8(4):137. http://doi.org/10.3390/min8040137

11. Li J, Sun Z, Wang L, Yang X, Zhang D, Zhang X, Wang M. 2022. Properties and mechanism of high-magnesium nickel slag-fly ash based geopolymer activated by phosphoric acid. Constr. Build. Mater. 345:128256 http://doi.org/10.1016/j.conbuildmat.2022.128256

12. Alshaaer M, Mallouh SA, Al-Kafawein J, Al-Faiyz Y, Fahmy T, Kallel A, Rocha F. 2017. Fabrication microstructural and mechanical characterization of luffa cylindrical fibre - reinforced geopolymer composite. Appl. Clay Sci. 143:125–133 http://doi.org/10.1016/j.clay.2017.03.030

13. Zhang B, Guo H, Yuan P, Deng L, Zhong X, Li Y, Wang Q, Liu D. 2020. Novel acid-based geopolymer synthesized from nanosized tubular halloysite: the role of precalcination temperature and phosphoric acid concentration. Cem. Concr. Compos. 110:103601. http://doi.org/10.1016/j.cemconcomp.2020.103601

14. Mabroum S, Garcia-Lodeiro I, El Machi A, Chhaiba S, Taha Y, Benzaazoua M, Blanco-Varela MT, Hakkou R. 2024. Acid resistance of alkali-activated binders based on clays from phosphate mining by-products. J. Build. Eng. 95:110106 http://doi.org/10.1016/j.jobe.2024.110106

15. El Machi A, Mabroum S, Taha Y, Tagnit-Hamou A, Benzaazoua M, Hakkou R. 2021. Use of flint from phosphate mine waste rocks as an alternative aggregates for concrete. Constr. Build. Mater. 271:121886 http://doi.org/10.1016/j.conbuildmat.2020.121886

16. En-Naji S, Mabroum S, Khatib K, Benzaazoua M, Hakkou R. 2023. Development of geopolymers from phosphate by-products for thermal insulation applications. Minerals 13(12):1480. http://doi.org/10.3390/min13121480

17. Mouih K, Hakkou R, Taha Y, Benzaazoua M. 2023. Performances of compressed stabilized bricks using phosphate waste rock for sustainable construction. Constr. Build. Mater. 388:131577. http://doi.org/10.1016/j.conbuildmat.2023.131577

18. Beniddar H, El Machi A, El Abbassi F.-E, Taha Y, Benzaazoua M, Hakkou R. 2024. Sustainable utilization of phosphate mine waste rocks as sand substitutes in cement mortar production. Constr. Build. Mater. 438:136949. http://doi.org/10.1016/j.conbuildmat.2024.136949

19. Seiffarth T, Hohmann M, Posern K, Kaps Ch. 2013. Effect of thermal pre-treatment conditions of common clays on the performance of clay-based geopolymeric binders. Appl. Clay Sci. 73:35–41. http://doi.org/10.1016/j.clay.2012.09.010

20. Fajnor V.Š, Jesenák K. 1996. Differential thermal analysis of montmorillonite. J. Therm. Anal. 46:489–493. http://doi.org/10.1007/BF02135026

21. Gunasekaran S, Anbalagan G. 2007. Thermal decomposition of natural dolomite. Bull. Mater. Sci. 30:339–344. http://doi.org/10.1007/s12034-007-0056-z

22. Belalem K, Benaboura A, Lerari D, Kanoun N, Chebout R. 2020. Effect of cationic and anionic clays as supports for styrene polymerization initiated by metallocenes/MAO catalytic system. Polym. Bull. 77:4289–4305. http://doi.org/10.1007/s00289-019-02941-6

23. Danner T, Norden G, Justnes H. 2018. Characterisation of calcined raw clays suitable as supplementary cementitious materials. Appl. Clay Sci. 162:391–402. http://doi.org/10.1016/j.clay.2018.06.030

24. Garg N, Skibsted J. 2019. Dissolution kinetics of calcined kaolinite and montmorillonite in alkaline conditions: evidence for reactive Al(V) sites. J. Am. Ceram. Soc. 102(12):7720–7734. http://doi.org/10.1111/jace.16663

25. Noushini A, Castel A, Aldred J, Rawal A. 2020. Chloride diffusion resistance and chloride binding capacity of fly ash-based geopolymer concrete. Cem. Concr. Compos. 105:103290. http://doi.org/10.1016/j.cemconcomp.2019.04.006

26. Wan Q, Zhang R, Zhang Y. 2022. Structure and properties of phosphate-based geopolymer synthesized with the Spent Fluid Catalytic-Cracking (SFCC) Catalyst. Gels. 8(2):130. http://doi.org/10.3390/gels8020130

27. Mabroum S, Aboulayt A, Taha Y, Benzaazoua M, Semlal N, Hakkou R. 2020. Elaboration of geopolymers based on clays by-products from phosphate mines for construction applications. J. Clean. Prod. 261:121317 http://doi.org/10.1016/j.jclepro.2020.121317

28. Flemming RL, Luth RW. 2002. ^{29}Si MAS NMR study of diopside–Ca-Tschermak clinopyroxenes: Detecting both tetrahedral and octahedral Al substitution. Am. Mineral. 87:25–36. http://doi.org/10.2138/am-2002-0104

29. Brouwer DH. 2023. 9.06 - Applications of silicon-29 NMR spectroscopy. In Comprehensive Inorganic Chemistry III (Third Edition); Reedijk J. Poeppelmeier KR. Eds, Elsevier: Oxford. pp. 107–137. ISBN 978-0-12-823153-1.

30. Tchakouté HK, Rüscher CH, Kamseu E, Andreola F, Leonelli C. 2017. Influence of the molar concentration of phosphoric acid solution on the properties of metakaolin-phosphate-based geopolymer cements. Appl. Clay Sci. 147:184–194. http://doi.org/10.1016/j.clay.2017.07.036

31. Şahin E, Çiftçioğlu M. 2014. Monetite promoting effect of citric acid on brushite cement setting kinetics. Mater. Res. Innov. 18:138–145. http://doi.org/10.1179/1433075X13Y.0000000175

32. Prado Da Silva MH, Lima JHC, Soares GA, Elias CN, de Andrade MC, Best SM, Gibson IR. 2001. Transformation of monetite to hydroxyapatite in bioactive coatings on titanium. Surf. Coat. Technol. 137(2-3):270–276. http://doi.org/10.1016/S0257-8972(00)01125-7

33. Arifuzzaman SM, Rohani S. 2004. Experimental study of brushite precipitation. J. Cryst. Growth. 267(3-4):624–634. http://doi.org/10.1016/j.jcrysgro.2004.04.024

34. Engstrand J, Persson C, Engqvist H. 2014. The effect of composition on mechanical properties of brushite cements. J. Mech. Behav. Biomed. Mater. 29:81–90 http://doi.org/10.1016/j.jmbbm.2013.08.024

35. Pu S, Zhu Z, Song W, Huo W, Zhang J. 2021. Mechanical and microscopic properties of fly ash phosphoric acid-based geopolymer paste: a comprehensive study. Constr. Build. Mater. 299:123947. http://doi.org/10.1016/j.conbuildmat.2021.123947

36. Riyap HI, Tazune FK, Fotio D, Tchakouté HK, Nanseu-Njiki CP, Rüscher CH. 2021. The coexistence of the poly(Phospho-Siloxo) networks and calcium phosphates on the compressive strengths of the acid-based geopolymers obtained at room temperature. J. Inorg. Organomet. Polym. Mater. 31:3301–3323. http://doi.org/10.1007/s10904-021-01949-8

37. Singh S, Singh V, Aggarwal S, Mandal UK. 2010. Synthesis of brushite nanoparticles at different temperatures. Chem. Pap. 64:491–498 http://doi.org/10.2478/s11696-010-0032-8

38. Li J, Zhang W, Lang L, Dong C, Huang K. 2024. Preparation and properties of geopolymer containing phosphoric acid-activated fly ash and mechanically-milled kaolinite: experiments and density function theory. J. Clean. Prod. 441:140992. http://doi.org/10.1016/j.jclepro.2024.140992

39. Liu D, Mao L, Wang H. 2019. Preparation of uniform newberyite crystal in nonaqueous system. Mater. Lett. 240:169–171 http://doi.org/10.1016/j.matlet.2019.01.016

40. Louati S, Baklouti S, Samet B. 2016. Geopolymers based on phosphoric acid and illito-kaolinitic clay. Adv. Mater. Sci. Eng. 2016(1):2359759 http://doi.org/10.1155/2016/2359759
41. Tchakouté HK, Bewa CN, Fotio D, Dieuhou CM, Kamseu E, Rüscher CH. 2021. Influence of alumina on the compressive strengths and microstructural properties of the acid-based geopolymers from calcined indurated laterite and metakaolin. Appl. Clay Sci. 209:106148. http://doi.org/10.1016/j.clay.2021.106148
42. Reig FB, Adelantado JVG, Moya Moreno MCM. 2002. FTIR Quantitative Analysis of calcium carbonate (calcite) and silica (quartz) mixtures using the constant ratio method. Application to geological samples. Talanta. 58(4):811–821. http://doi.org/10.1016/S0039-9140(02)00372-7
43. Lin H, Liu H, Li Y, Kong X. 2021. Properties and reaction mechanism of phosphoric acid activated metakaolin geopolymer at varied curing temperatures. Cem. Concr. Res. 144:106425. http://doi.org/10.1016/j.cemconres.2021.106425
44. Yu Y, Guo H, Pujari-Palmer M, Stevensson B, Grins J, Engqvist H, Edén M. 2019. Advanced solid-state 1H/31P NMR characterization of pyrophosphate-doped calcium phosphate cements for biomedical applications: the structural role of pyrophosphate. Ceram. Int. 45(16):20642–20655. http://doi.org/10.1016/j.ceramint.2019.07.047
45. Wang Q, Nielsen UG. 2020. Applications of solid-state NMR spectroscopy in environmental science. Solid State Nucl. Magn. Reson. 110:101698. http://doi.org/10.1016/j.ssnmr.2020.101698
46. Wang YS, Alrefaei Y, Dai JG. 2020. Influence of coal fly ash on the early performance enhancement and formation mechanisms of silico-aluminophosphate geopolymer. Cem. Concr. Res. 127:105932. http://doi.org/10.1016/j.cemconres.2019.105932